Supporting Information

Kinetics and Pore Formation of the Sodium Metal Anode on NASICON-Type $Na_{3.4}Zr_2Si_{2.4}P_{0.6}O_{12}$ for Sodium Solid-State Batteries

Till Ortmann, Simon Burkhardt, Janis Kevin Eckhardt, Till Fuchs, Ziming Ding, Joachim Sann, Marcus Rohnke, Qianli Ma, Frank Tietz, Dina Fattakhova-Rohlfing, Christian Kübel, Olivier Guillon, Christian Heiliger, and Jürgen Janek*

Supplementary Information

Kinetics and Pore Formation of the Sodium Metal Anode on NASICON-type $Na_{3.4}Zr_2Si_{2.4}P_{0.6}O_{12}$ for Sodium Solid-State Batteries

Till Ortmann, Simon Burkhardt, Janis Kevin Eckhardt, Till Fuchs, Ziming Ding, Joachim Sann, Marcus Rohnke, Qianli Ma, Frank Tietz, Dina Fattakhova-Rohlfing, Christian Kübel, Olivier Guillon, Christian Heiliger and Jürgen Janek*

Mr. T. Ortmann, Dr. S. Burkhardt, Mr. T. Fuchs, Dr. J. Sann, Dr. M. Rohnke and Prof. J. Janek
Institute for Physical Chemistry, Justus Liebig University Giessen, 35392 Giessen, Germany.
*E-Mail: juergen.janek@phys.chemie.uni-giessen.de

Mr. T. Ortmann, Dr. S. Burkhardt, Mr. J. K. Eckhardt, Mr. T. Fuchs, Dr. J. Sann, Dr. M. Rohnke, Prof. C. Heiliger and Prof. J. Janek
Center for Materials Research (ZfM), Justus Liebig University Giessen, 35392 Giessen, Germany.

Mr. J. K. Eckhardt, Prof. C. Heiliger
Institute for Theoretical Physics, Justus Liebig University Giessen, 35392 Giessen, Germany.

Ms. Z. Ding and Prof. C. Kübel
Technische Universität Darmstadt, 64289 Darmstadt, Germany.

Dr. Q. Ma, Dr. F. Tietz, Prof. D. Fattakhova-Rohlfing and Prof. O. Guillon
Forschungszentrum Jülich GmbH, Institute of Energy and Climate Research, Materials Synthesis and Processing (IEK-1), 52425 Jülich, Germany.

Ms. Z. Ding and Prof. C. Kübel
Institute of Nanotechnology (INT) and Helmholtz Institute Ulm (HIU), Karlsruhe Institute of Technology (KIT), 76344 Eggenstein-Leopoldshafen, Germany.

Prof. D. Fattakhova-Rohlfing
Department of Engineering and Center for Nano integration Duisburg-Essen (CENIDE), Universität Duisburg-Essen, 47057 Duisburg, Germany.

Prof C. Kübel
Karlsruhe Nano Micro Facility (KNMF), Karlsruhe Institute of Technology (KIT), 76344 Eggenstein-Leopoldshafen, Germany.

Prof. O. Guillon
Jülich Aachen Research Alliance, JARA-Energy, 52425 Jülich, Germany.

1. Materials characterization

a)
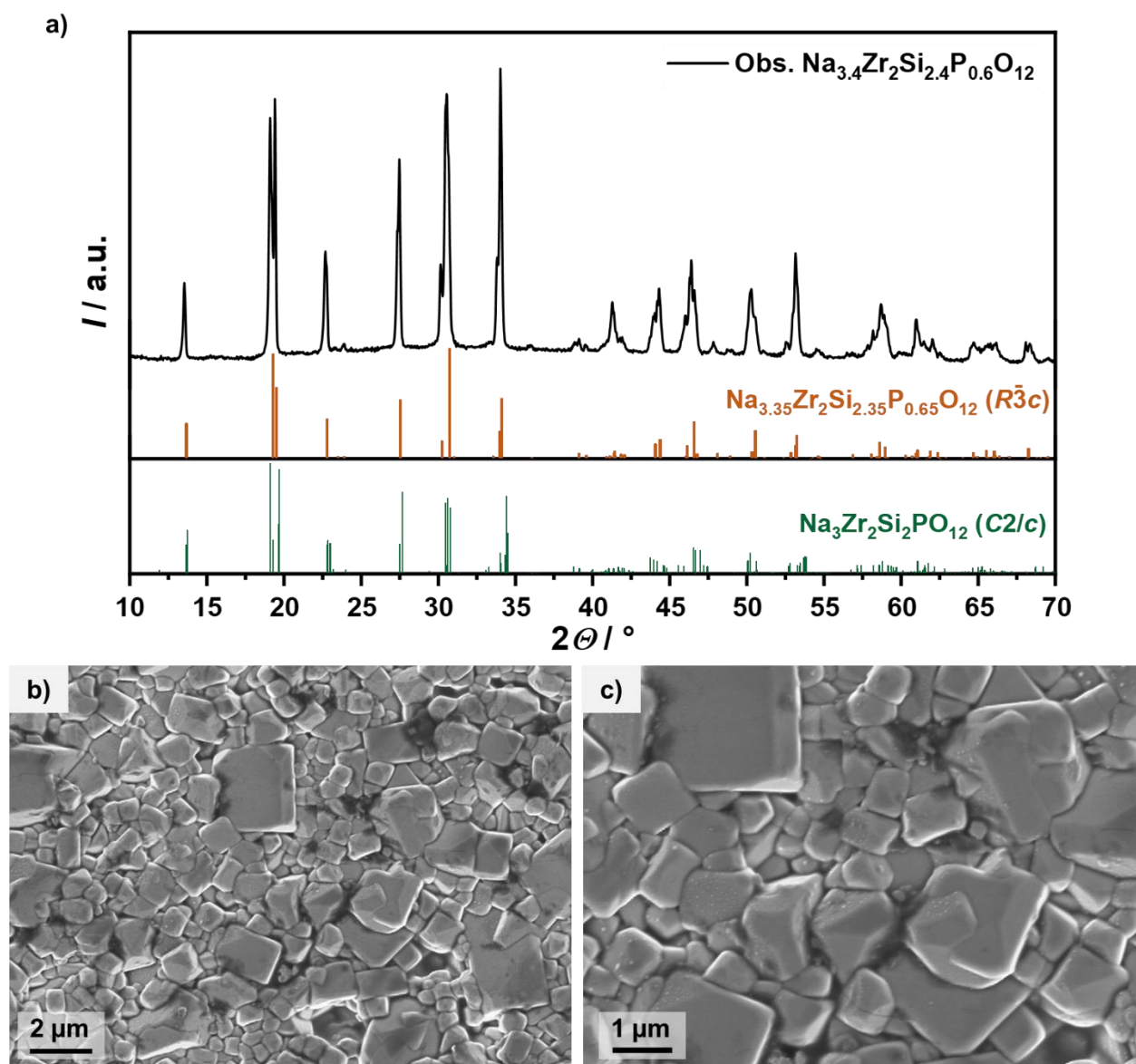
Figure S-1: *a) XRD pattern of the synthesized $Na_{3.4}Zr_2Si_{2.4}P_{0.6}O_{12}$ solid electrolyte in comparison to the reference patterns of $Na_3Zr_2Si_2PO_{12}$ (C2/c, ICSD000473) and $Na_{3.35}Zr_2Si_{2.35}P_{0.65}O_{12}$ ($R\bar{3}c$, ICSD 062386). SEM image of the pristine surface of sintered $Na_{3.4}Zr_2Si_{2.4}P_{0.6}O_{12}$ at b) low magnification and c) at higher magnification. A crystalline surface with a grain size distribution between about 0.4 μm and 3 μm is visible.*

Based on X-ray diffraction (XRD) analysis, NZSP0.4 solid electrolyte including monoclinic and rhombohedral phase was obtained and used for all experiments (**Figure S-1a**). SEM images indicate a crystalline surface of the material (**Figure S-1b** and **c**). Based on the macroscopic dimensions of the NZSP0.4 separators investigated, the relative density of the separator was >95 %.

2. Impedance analysis of $Na_{3.4}Zr_2Si_{2.4}P_{0.6}O_{12}$
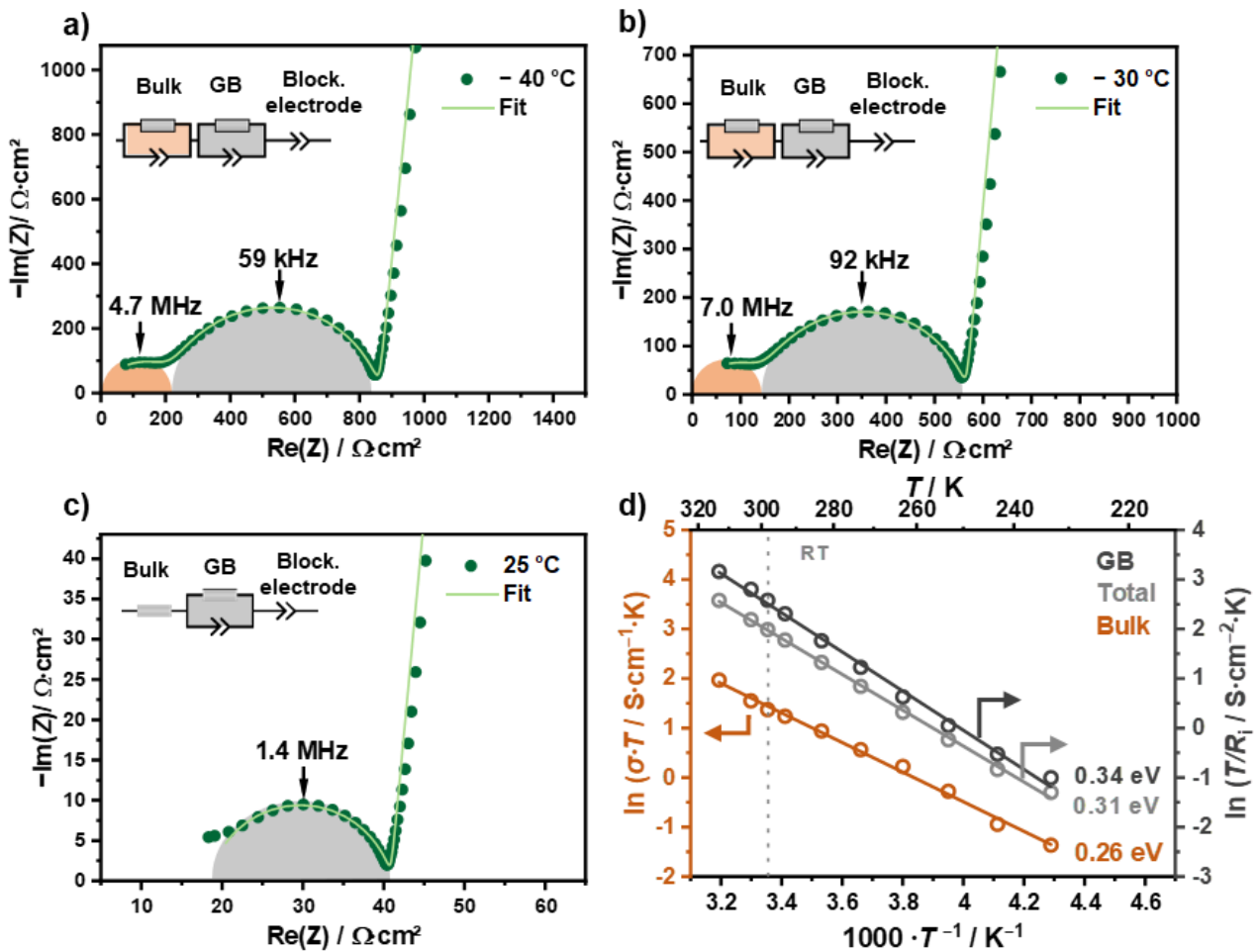
Figure S-2*: Impedance spectra of a symmetric Au|NZSP0.4|Au cell at a) − 40 °C b) − 30 °C and c) 25 °C. The frequency of the bulk contribution shifts outside the measurement range with increasing temperature. Therefore, at temperatures above − 30 °C the bulk is described by a resistance instead of an RQ element. At 25°C, no bulk contribution is observed within the selected frequency range. d) Arrhenius plot and determined activation energy for bulk and grain boundary transport in the temperature range of −40 and 40 °C. For the bulk process the ionic conductivities are shown whereas for grain boundaries only the resistance in dependence of temperature is visualized.*

To characterize the bulk and grain boundary transport processes of the NZSP0.4, impedance analysis of symmetric Au|NZSP0.4|Au cells at different temperatures were recorded and are shown in **Figure S-2a-c**. At −40 °C two separated semicircles are observed in the high- and mid-frequency range with apex frequencies at 4.7 MHz and 59 kHz. In the low-frequency range a strong increase of impedance is obtained. The process at high frequencies (f_{apex}(−40 °C) = 4.7 MHz) is assigned to the bulk transport while the process in the mid-frequency range (f_{apex}(−40 °C) = 59 kHz) is attributed to grain boundary transport, which is in accordance with literature.[1,2] The pronounced polarization at low frequencies is caused by the blocking behavior of the gold electrodes.[3] By elevating the temperature, the apex frequency of bulk transport shifts to higher frequencies ($f_{apex,bulk}$(−30 °C) = 7.0 MHz) and is beyond the measured frequency range at 25 °C. At elevated

3

temperature the bulk transport is therefore modeled by a serial resistance instead of an *RQ*-element in the equivalent circuit.

Based on the *brick layer model*[2] activation energies for bulk and GB transport process of $E_{a,bulk}$ = 0.26 eV and $E_{a,GB}$ = 0.34 eV were determined. The total activation energy $E_{a,tot}$ = 0.31 eV (for combined bulk and GB resistance) is in good agreement with the literature value for NZSP0.4, whereas a slightly lower $E_{a,bulk}$ = 0.28 eV is reported.[3] The measurement has been repeated and the mean activation energy for bulk, GB and total transport are summarized in **Table S-4.**

The ionic conductivity of the bulk can be calculated by the following equation:

$$\sigma_{bulk} = \frac{L}{A \cdot R_{bulk}} \qquad \text{(E1)}$$

With the thickness *L* of the SE pellet, the electrode area *A* and the measured resistance of the bulk R_{bulk} from impedance analyses an ionic conductivity for bulk transport σ_{bulk} = 1.1 mS·cm^{-1} at −40 °C is obtained. Calculating the GB conductivity σ_{GB} by **Equation 1** is not correct since the volume fraction of the GB is much smaller compared to the volume fraction of the grains in the SE pellet.[4] Hence, for determine σ_{GB} the respective capacitance for bulk C_{bulk} and GB C_{GB} must be considered according to **Equation 2**:

$$\sigma_{GB} = \frac{L}{A} \left(\frac{C_{bulk}}{C_{GB}} \right) \frac{1}{R_{GB}} \qquad \text{(E2)}$$

As the C_{bulk} is necessary for determination, σ_{GB} can only calculated for low temperature as $f_{apex,bulk}$ shifts beyond the measured frequency range. At −40 °C a σ_{GB} = 0.014 mS·cm^{-1} is obtained. However, due to this limitation **Figure S-2d** only shows the temperature dependence of R_{GB} obtained from the respective impedance spectra.

3. Temperature-correction for time-resolved impedance analysis of Na|NZSP0.4 interface
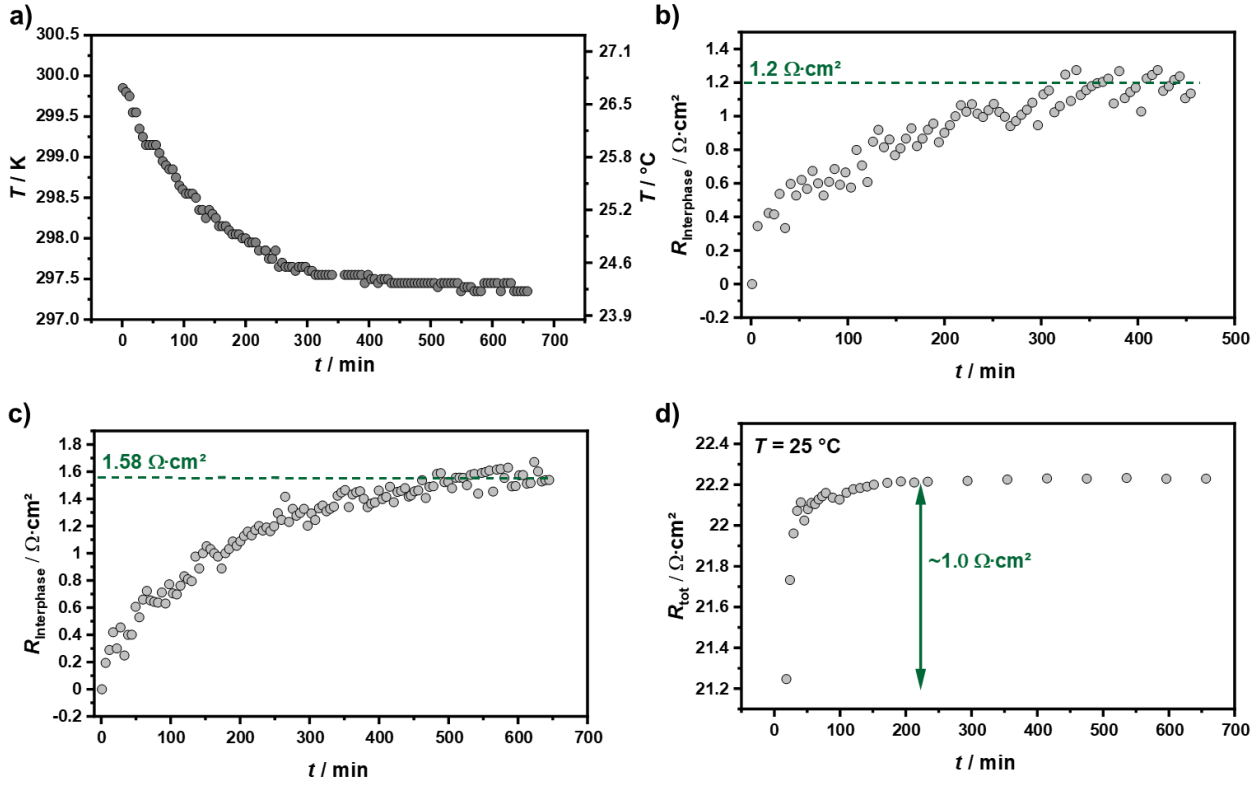
Figure S 3: a) Temperature profile during time-resolved impedance analysis inside the glovebox. The thermocouple was placed directly next to the electrochemical cell. Representation of the temporal evolution of $R_{\text{Interphase}}$ for two independent measurement series shown in b) and c), which have already been corrected for temperature fluctuations during the impedance recording. d) Real part of total resistance of a symmetric Na|NZSP0.4|Na cell at a constant temperature of 25°C as function of time. Time delay between assembly and recording was roughly 18 minutes.

Figure S-3a shows the temperature profile of the glovebox during impedance analysis indicating a temperature decrease of roughly 2.5 °C. To compensate for temperature changes during measurements we subtracted a correction term R_{Corr} from the measured real part of impedance R_{m} and obtain the real part of resistance of the growing interphase $R_{\text{Interphase}}$ (E3):

$$R_{\text{Interphase}} = R_{\text{m}} - R_{\text{Corr}} \qquad \text{(E3)}$$

R_{Corr} has been calculated based on the temperature dependence of the ionic conductivity of NZSP0.4, which is described in the following:

The ionic conductivity in solid electrolytes can be described using **Equation E4**:[5]

$$\sigma \cdot T = \sigma_0 \cdot \exp\left(\frac{-E_{\text{a}}}{k_{\text{B}} T}\right) \qquad \text{(E4)}$$

were σ describes the conductivity, E_{a} the activation energy, T the absolute temperature and k_{B} the Boltzmann constant. σ_0 is the pre-exponential factor which includes crystallographic properties of

the material under consideration. Since the specific conductivity is proportional to the reciprocal resistance, **Equation E4** can be transformed to:

$$\frac{T}{R} = \frac{1}{R_0} \cdot \exp\left(\frac{-E_a}{k_B T}\right) \tag{E5}$$

Rearrangement of **Equation E5** leads to:

$$R(T) = T \cdot R_0 \cdot \exp\left(\frac{E_a}{k_B T}\right) \tag{E6}$$

If the activation energy E_a and the constant R_0 are known for a material or a specific sample, the resulting resistance R can be calculated for any temperature.

In case of time-dependent impedance analysis, this relationship (**Equation E6**) was used to calculate the influence of temperature fluctuations inside the glovebox on the resistance (ionic conductivity) of NZSP0.4. It is assumed that the temperature only influences the conductivity of the solid electrolyte and not that of a (possible) formed interphase. By means of symmetrical Au|NZSP0.4|Au cells the activation energy for bulk and grain boundary transport was determined as 0.244 eV and 0.357 eV, respectively. These values were obtained from two different cells. The pre-exponential Factor R_0^{-1} is sample-dependent and therefore cannot be taken from measurements with blocking electrodes.

For the determination of R_0 it is assumed that the first recorded impedance spectrum of a measurement series has not yet formed an interlayer. In this case the impedance spectrum contains only the bulk and grain boundary properties of the solid electrolyte. By fitting this first impedance spectrum using an $R_{bulk}-R_{GB}Q_{GB}$ equivalent circuit, the resistance of bulk $R_{bulk,t=0}$ and grain boundary $R_{GB,t=0}$ at time $t = 0$ were determined. Based on these resistances combined with the activation energies $E_{a,bulk}$ and $E_{a,GB}$ as well as the temperature T, R_0 were calculated for bulk and grain boundary transport.

$$R_{0,bulk} = \frac{R_{bulk,t=0}}{T} \cdot \exp\left(\frac{-E_{a,bulk}}{k_B T}\right) \tag{E7}$$

$$R_{0,GB} = \frac{R_{GB,t=0}}{T} \cdot \exp\left(\frac{-E_{a,GB}}{k_B T}\right) \tag{E8}$$

With the help of the determined factors $R_{0,bulk}$ and $R_{0,GB}$ and the respective activation energies for bulk $E_{a,bulk}$ and grain boundary transport $E_{a,GB}$, the resistance of a specific sample can be calculated as a function of temperature.

$$R_{bulk}(T) = R_{0,bulk} \cdot T \cdot \exp\left(\frac{E_{a,bulk}}{k_B T}\right) \tag{E9}$$

$$R_{\text{GB}}(T) = R_{0,\text{GB}} \cdot T \cdot \exp\left(\frac{E_{a,\text{GB}}}{k_B T}\right) \tag{E10}$$

The addition of $R_{\text{bulk}}(T)$ and $R_{\text{GB}}(T)$ gives the corrected total resistance of the solid electrolyte at a given temperature.

$$R_{\text{Corr}}(T) = R_{\text{bulk}}(T) + R_{\text{GB}}(T) \tag{E11}$$

It must be taken into account that with the described temperature correction a relative error for R_{Corr} of about 50 % is obtained. This is mainly due to the absolute errors of the determined activation energies of bulk and GB obtained from the linear regression. Since the values of R_{Corr} and R_m are close to each other, extremely high absolute errors of a factor of 10 result for $R_{\text{Interphase}}$.

4. XPS Analysis of Na|NZSP0.4 Interface
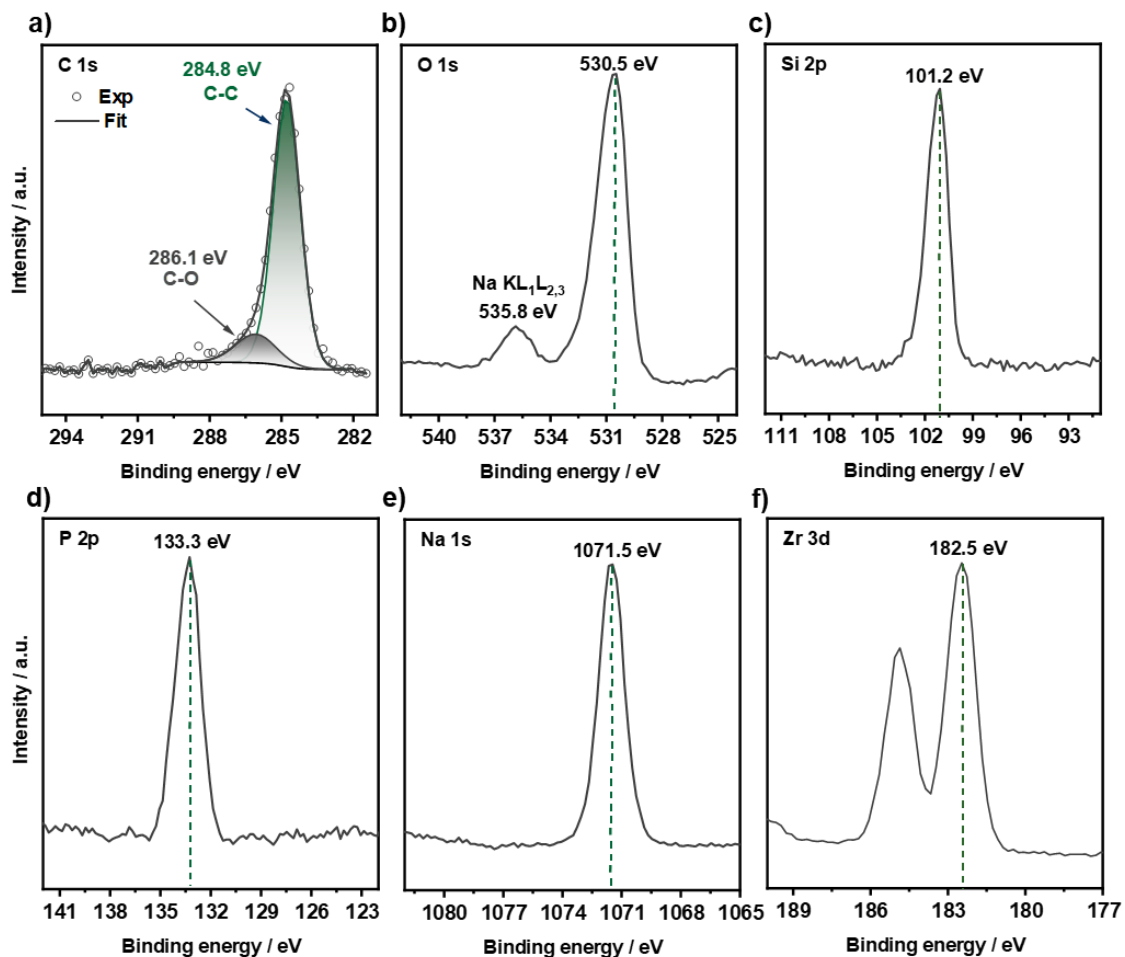
Figure S-4: *Detail XP spectra of a) C 1s, b) O 1s, c) Si 2p, d) P 2p, e) Na 1s and f) Zr 3d of an untreated pristine $Na_{3.4}Zr_2Si_{2.4}P_{0.6}O_{12}$ surface.*
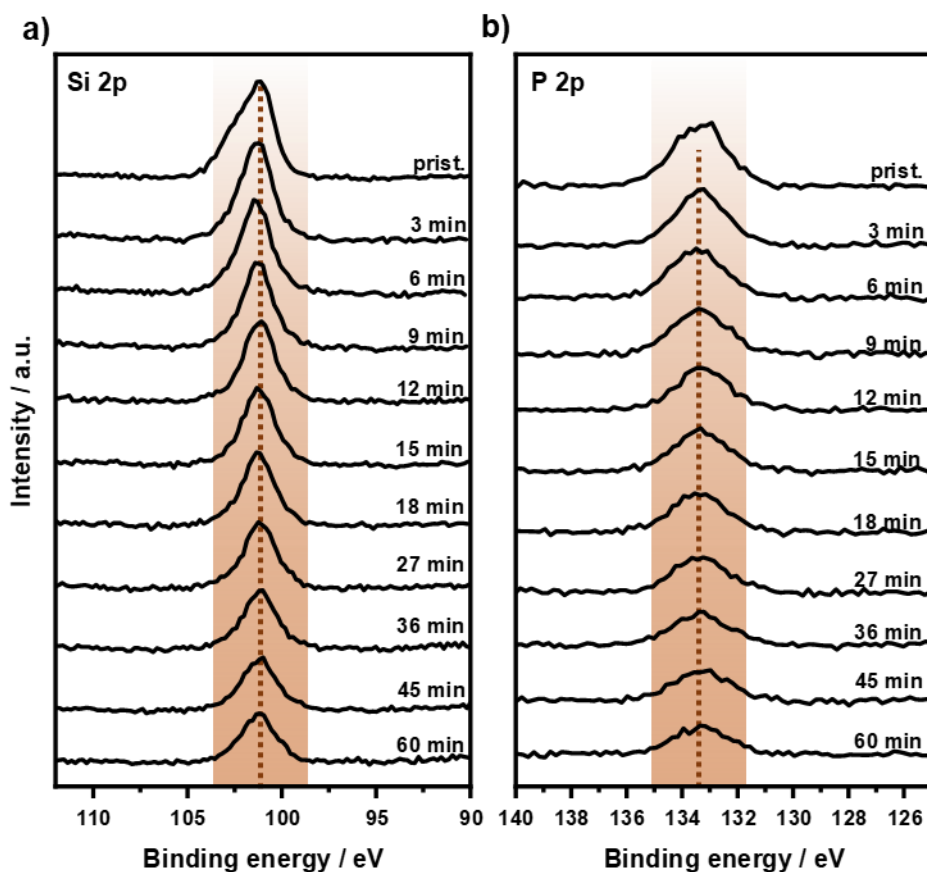
Figure S-5: XP spectra of a) Si 2p and b) P 2p lines after deposition of different amounts of sodium. No changes in binding energy are observed for both signals. Thus, Si and P are not reduced in contact with sodium or decomposition products are formed that are either volatile or react further with the chamber atmosphere and cannot be detected by XPS.
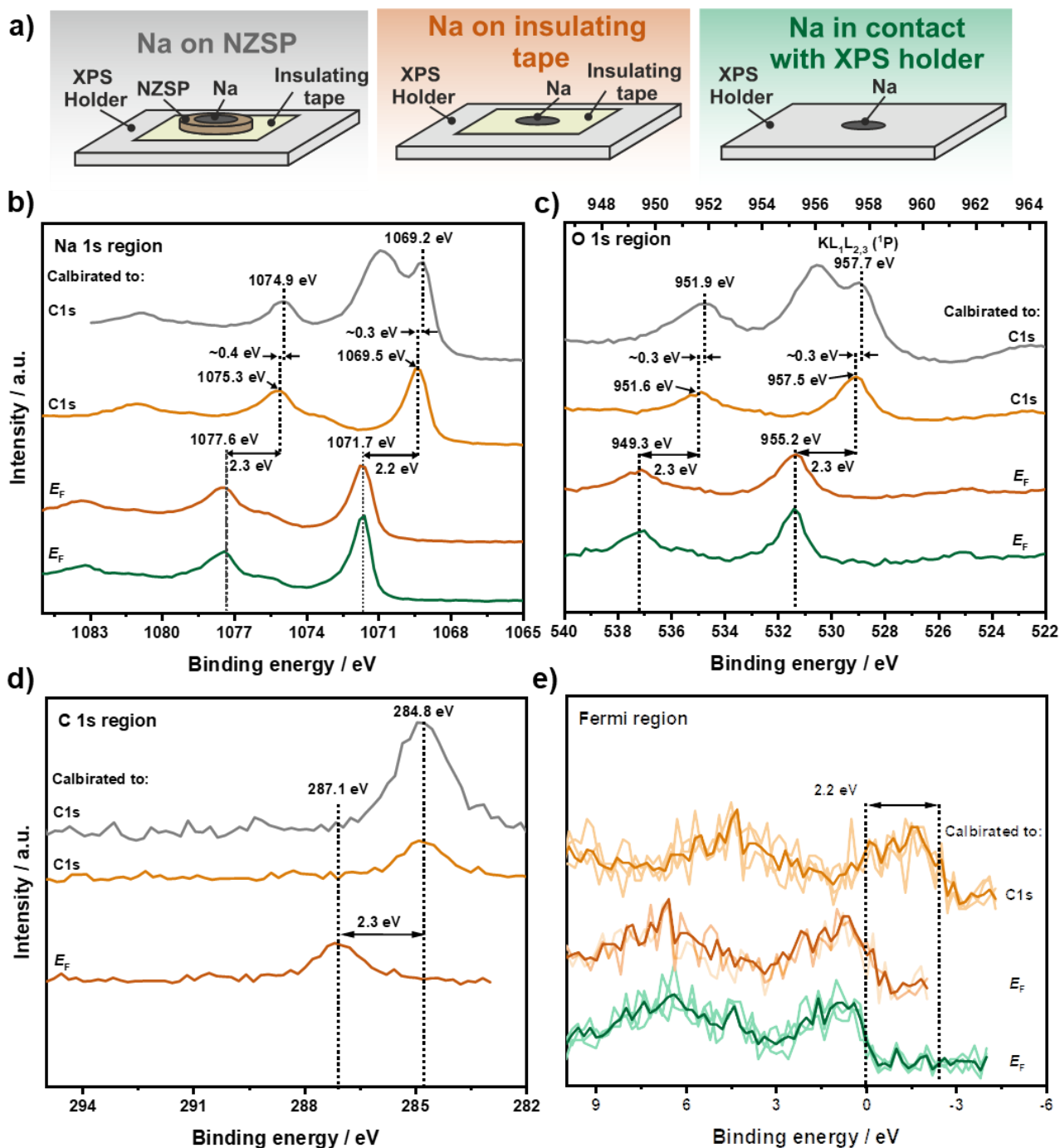
***Figure S-6**: Overview of sodium XP spectra at different boundary conditions. Three different measurements were performed with different measurement settings (with and without dual beam neutralization) and measurement setups. a) Sketch of the measurement setups used. Neutralization was used for samples fixed on insulating tape. These spectra are calibrated with the C 1s signal (grey and light orange curves). Additionally, the measurement of sodium metal with neutralization is calibrated to the Fermi level for better comparison, too (dark orange curves). Sodium in direct contact with the sample holder was measured without neutralization and calibrated to Fermi level (green curves). b)-e) XP spectra of Na 1s, O 1s, C 1s and Fermi region for the respective measurement conditions. For the Fermi region, three measurements for each condition (light tint) and the corresponding average value (dark tint) are shown. Independent of the measurement method (with or without neutralization), identical spectra are obtained for sodium metal when calibrating to the Fermi level. However, when an electrically insulating layer between the sodium*

and the sample holder is present and the spectra are calibrated on C 1s signal, a clear shift of roughly 2.5 eV of all sodium signals including the Fermi level to lower energies can be observed compared to the sodium samples directly contacted to the sample holder. The shift indicates that an equilibration of the Fermi levels is not possible when an insulation layer is present between sample and sample holder.

To the best of our knowledge, only the energy loss of bulk and surface plasmon excitation is known in the literature, but not a suitable fit model for the Na 1s signal or Na Auger emission in the O 1s region for sodium metal.[6] However, to determine the shift of the sodium metal signals in the Na 1s and O 1s region for the different measurement settings, a simplified fit model was designed. We would like to emphasize that the presented fit model is not an ideal description of the Na 1s and Na Auger emission for sodium metal, but it is sufficient to identify relative changes between different measurement conditions.

The presented Na 1s spectrum for sodium metal should contain the main peak as well as the first and second excitations of bulk and surface plasmon. For simplification, all components are assigned to a Gaussian-Lorentzian function (GL(30)) for peak description. In addition, the corresponding energy spacings of the plasmon excitations and full-width-half-maximum < 2 were used as constraints for fitting. A further component was added to the model describing Na^+-species originating from NZSP0.4 and possible sodium containing degradation products, when the sodium metal was deposited on the SE.

For fitting the O 1s region, the Na^0-$KL_1L_{2,3}$ transition with first bulk and surface plasmonic excitation were considered for sodium metal. Analogous to the fitting of the Na1s spectrum, an identical function and constraints were used for the components. For the case of sodium in contact with NZSP0.4, one further component was added describing the oxygen component of the SE. Further Auger signals originating from Na^+ species were neglected. The obtained parameters for Na 1s and O 1s regions of the different measurements are summarized in Figure S-6 and **Table S-1** and **S-2**.
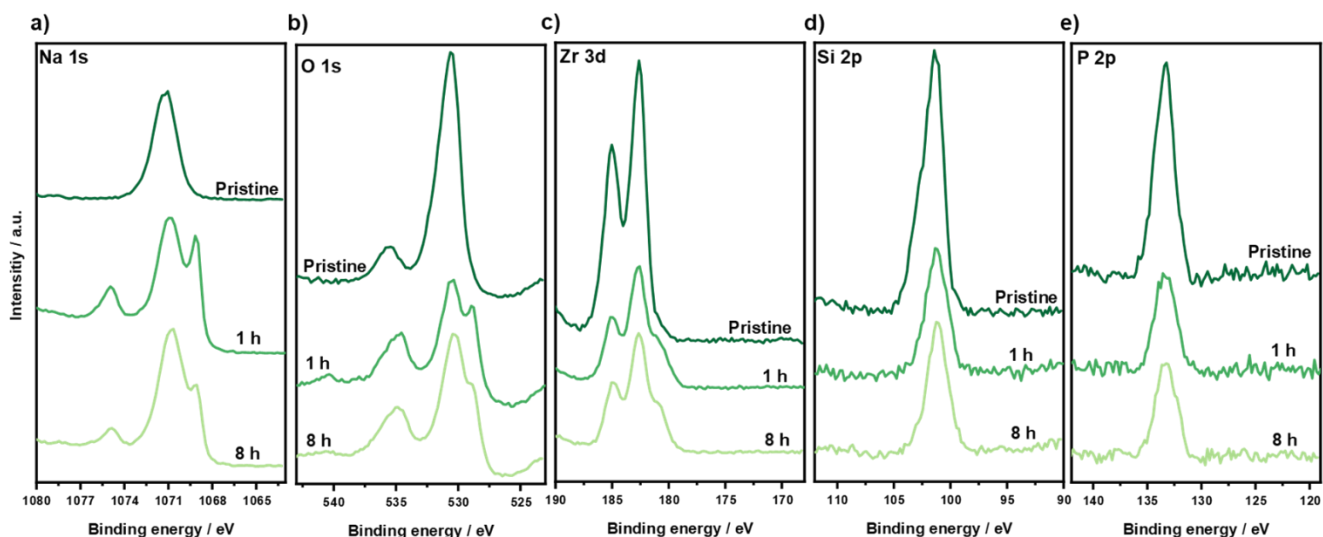
Figure S-7*: XP Spectra of the solid electrolyte before sodium deposition, after a total deposition time of 1 h and after 8 h of the last deposition cycle. Except for the decrease of the sodium metal signals in the Na 1s and O 1s regions, only the Zr 3d signal profile shows a shoulder at 181.0 eV after sodium deposition.*

5. Transmission electron microscopy of Na|NZSP0.4 interface
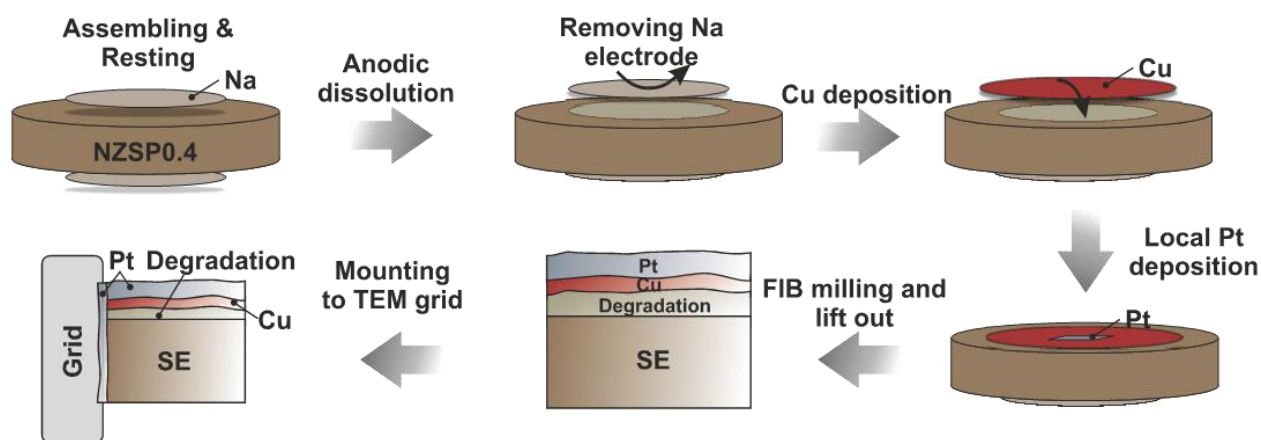
Figure S-8*: a) Illustration of preparation route of electron transparent specimen for TEM characterization. A tight copper layer was deposited on the NZSP0.4 after removing the sodium electrode to protect the exposed surface. For preparation of the electron transparent specimen and mounting on the TEM grid, deposition of platinum was used.*
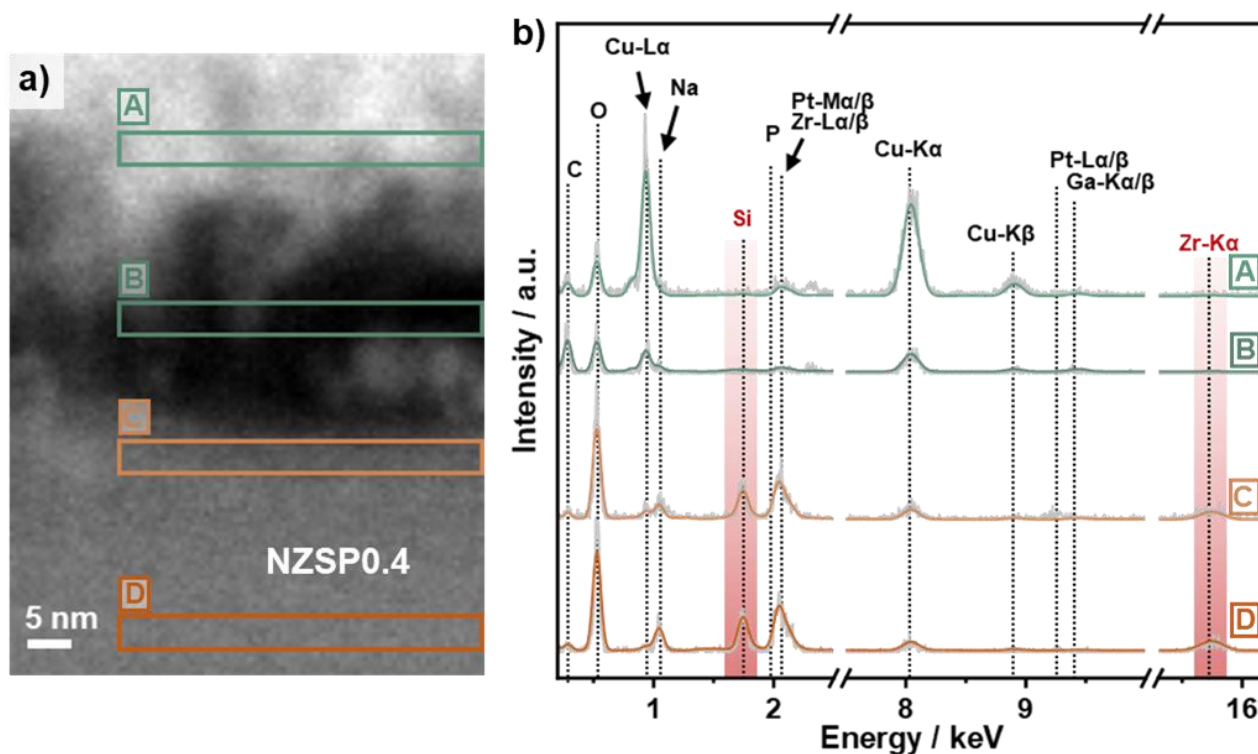
Figure S-9*: a) HAADF-STEM image of a prepared electron transparent lamella from the Na|NZSP0.4 interface. Based on different morphologies, the NZSP0.4 solid electrolyte separates clearly from the deposit protection layer. b) EDX spectra of selected regions which are highlighted in green and orange in b). The measured spectra are shown in light grey while the model spectra are presented in the respective color (orange and green). Similar to the results shown in **Figure 3**, no obvious changes of the elemental composition in the bulk and near-surface region of the NZSP0.4 are obtained. The present of copper signal inside the NZSP0.4 region is probably caused by the cryo transfer holder system. The protection layer consists mainly of copper and small amounts of platinum. In addition, the present of sodium and oxygen in the protection layer originate from the degradation of residual sodium which have not removed with the bulk sodium electrode.*

6. Normalization of impedance spectra with different geometric electrode areas

For comparing impedance spectra obtained from cells with different electrode size a normalization to the geometric electrode area is not sufficient, since the volume contribution to the overall conductivity of the SE changes, too. This is the case when sodium is gradually attached to an SE by applying a uniaxial force where beside an improvement of interfacial contact also the geometric electrode area increases. In other words, the dynamic constriction (improvement of interfacial contact) is superimposed by a static constriction (change of electrode area) effect.[7] To account for the static constriction effect in the normalization, the ionic bulk conductivity $\sigma_{SE,bulk}$ of the SE can be used. Since the geometric thickness d and $\sigma_{SE,bulk}$ are constant during the experiment, the electrode area $A_{El,cal}$ can be calculated using the fitted series resistor R_{Ser} according to:

12

$$A_{\text{El,cal}} = \frac{d}{\sigma_{\text{SE}} \cdot R_{\text{Ser}}} \tag{E12}$$

This calculated electrode area can be used to normalize the impedance spectra as well as the resistances and capacitances determined from the spectra.

7. Distribution of relaxation times of symmetric Na|NZSP0.4|Na cells
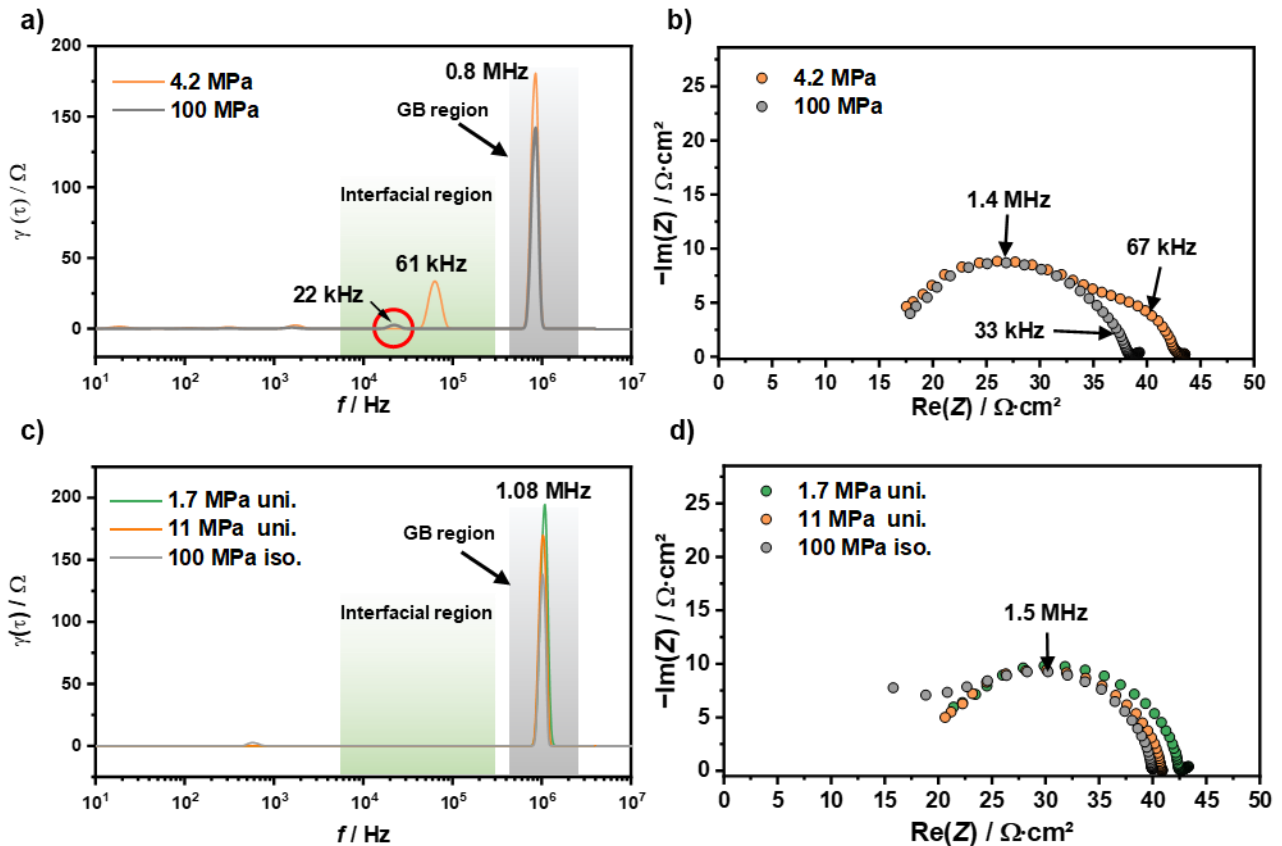
Figure S-10: *a) Representation of selected DRT analyses of the symmetrical cell Na$_{bc}$|NZSP0.4|Na$_{id}$, where the working electrode was pressed on the SE step by step with increasing force/pressure. Shown are the cases after an applied pressure of 4.2 MPa (215 N) and 100 MPa. For comparison, the corresponding Nyquist plots are shown in b). The green background indicates the region in which interface-related signals are expected in the DRT analysis while the grey background indicates the grain boundary region. In both cases, two signals (22 kHz and 61 kHz) are present in this interface-related region, although after a pressure of 100 MPa this is markedly less pronounced (Figure a, outlined in red). c) DRT analyses of Na$_{bc}$|NZSP0.4|Na$_{id}$ cells assembled at three different pressures with the corresponding Nyquist plots in d). In contrast to a), for the sodium working electrodes shown in c) only one pressure step was performed at the indicated pressures. For all three cells, no signal indicating an interfacial contribution was obtained in the DRT analysis (c and d).*

8. Activation energies of Na|NZSP0.4|Na cells with different interfacial contact
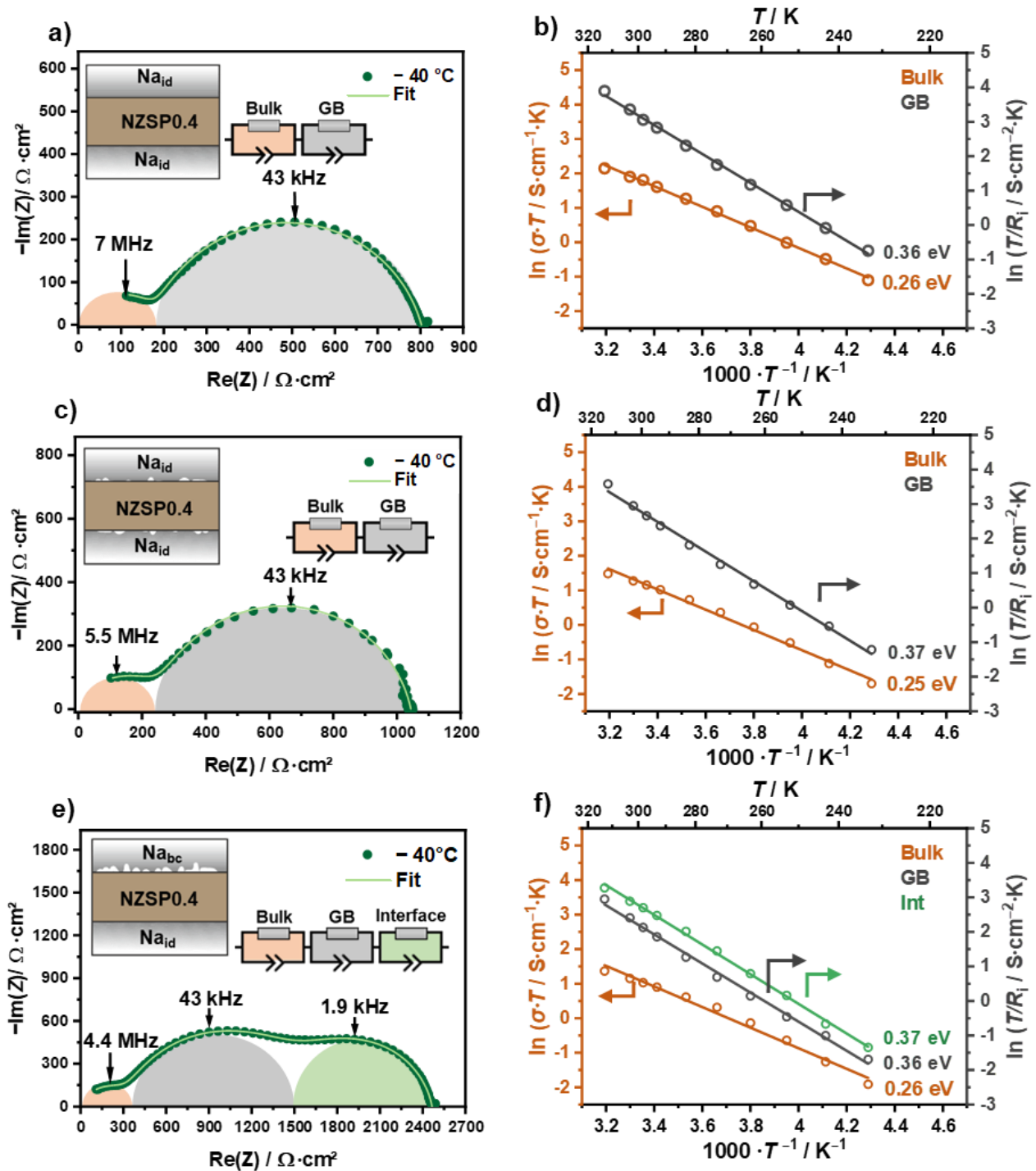
Figure S-11: *Impedance data (left column) and associated Arrhenius plots (right column) of three Na|NZSP0.4|Na cells which have been assembled with different protocols of attaching the sodium electrodes. The abbreviations "bc" stand for low and "id" ideally reversible electrode. For all cells impedance data at − 40 °C are shown in the left column. Determined activation energies of different processes (bulk, GB and interface) are inserted in the Arrhenius plots for each cell, respectively. For the bulk process the ionic conductivities are shown whereas for grain boundaries and interface process only the resistance in dependence of temperature are visualized.*

Three Na|NZSP0.4|Na cells with different interfacial contact were analyzed by temperature-dependent impedance analysis to determine the activation energies for the bulk, GB, and interface transport processes. Impedance spectra for each cell at −40 °C are on the right-hand side in **Figure S-11** where the corresponding Arrhenius plots are shown on the left-hand side. Starting with an ideal interfacial contact (Figure S-9a) even at low temperatures in the high- and mid-frequency range only bulk and GB transport are observed. No additional interfacial contribution is observed. Furthermore, the apex frequencies as well as the values for $E_{a,bulk} = 0.26$ eV and $E_{a,GB} = 0.36$ eV are very similar to those obtained from Au|NZSP0.4|Au cells (see **Table S-4**). Contributions from the interface including the formed interphase are negligibly small.

Even when small pores are present (< 100 nm, compare Figure 4d and e) at the interface, only the bulk and GB contributions are found at −40 °C in the respective impedance (Figure S-11c). Similar to the previous case values for $E_{a,bulk}$ and $E_{a,GB}$ are close to those determined in Au|NZSPO0.4|Au cells (see Figure S-11d and Table S-4). Based on this result the prepared electrode can be considered as a QRE.

The WE was then attached using a much lower external load while a QRE was used as counter electrode. Beside bulk and GB processes in the high- and mid-frequency range a clear contribution at 1.4 kHz with $C_{Int} = 0.1$ µF·cm^{-2} is observed (Figure S-11e) which we can safely attribute to the interface. For the interfacial contribution an activation energy $E_{a,Int} = 0.37$ eV is determined, which is close to $E_{a,GB}$ (Figure S-11f). All determined E_a are summarized in Table S-4.

9. Anodic dissolution of Na|NZSP0.4|Na inside SEM chamber ($p = 10^{-3}$ Pa)
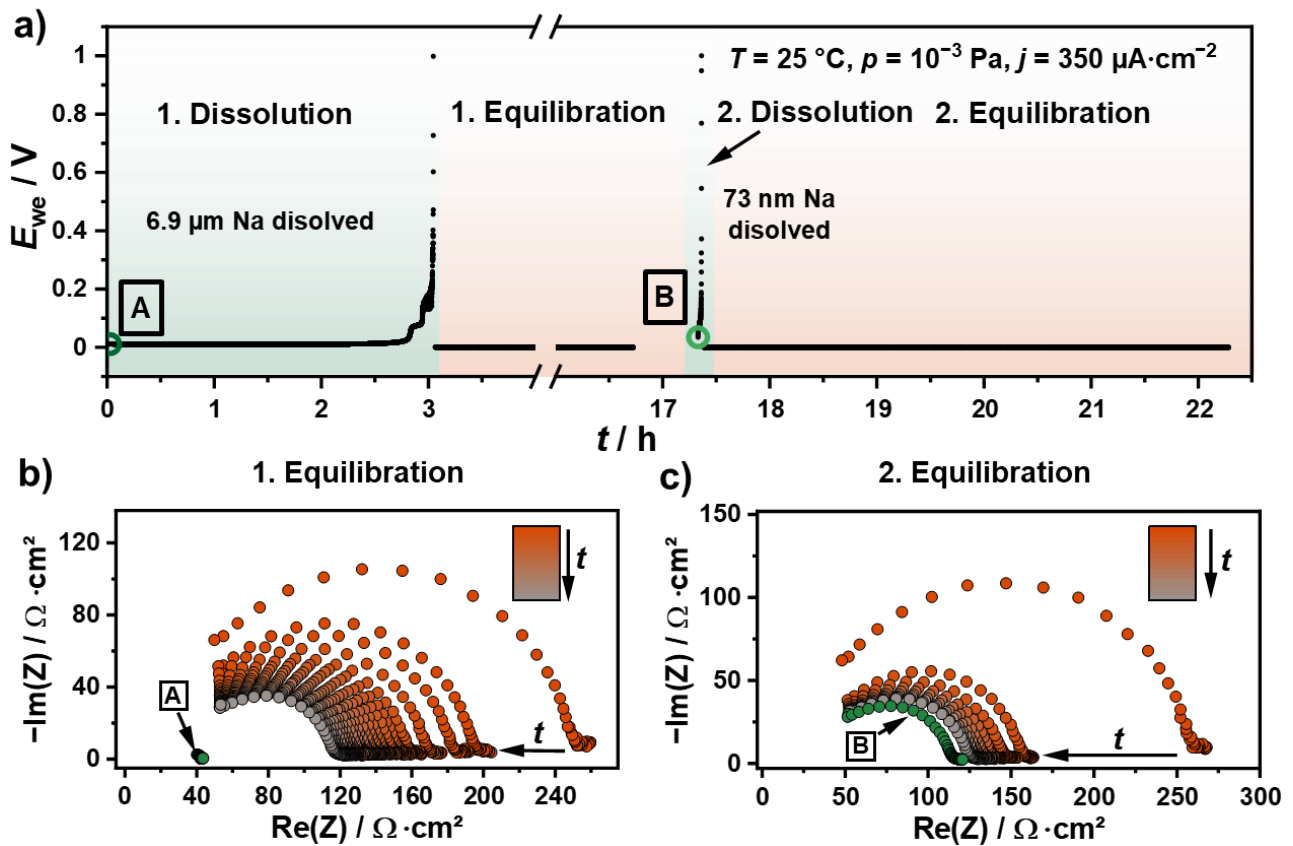
Figure S-12: *a) Chronopotentiometric curve of a symmetrical $Na_{idR}/NZSP0.4/Na_{idR}$ cell at a current density of 350 µA·cm^{-2} and at a pressure of 10^{-3} Pa. After reaching the cut-off voltage of 1V, the electrode was analyzed by PEIS in intervals of 5 minutes until the changes of the real part of the resistance were less than 1 Ω·cm². The described procedure was repeated again with the same electrode. With the first dissolution around 6.9 µm of sodium was resolved, whereas with the second dissolution only 73 nm could be dissolved. b) Development of impedance during the equilibration period of the anodically dissolved electrode. In green, the pristine impedance is inserted in the figure (also shown in figure a) at point A. A decrease in impedance is also observed in the vacuum, but it does not reach the pristine state. c) Nyquist plot of the second equilibration period.*

10. Schematic illustration of preparation of symmetrical Na|NZSP0.4|Na$_{id}$ cells
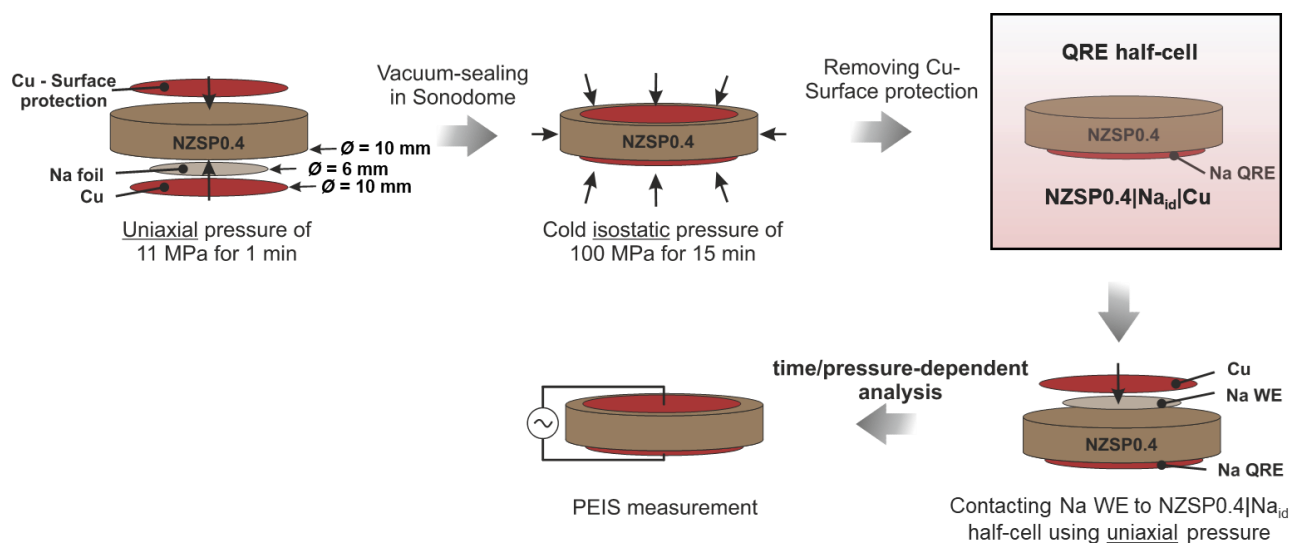
Figure S-13*: Schematic illustration of the preparation process of a quasi-reference (QRE) sodium electrode for a NZSP0.4/Na$_{id}$ half-cell. Na$_{id}$ denotes an ideally reversible sodium electrode. A copper foil is used for easier handling and protection against degradation of the sodium foil inside the glovebox. For time-dependent analysis the NZSP0.4/Na$_{id}$ half-cell is complemented with a working electrode (WE) by pressing a sodium foil at 11 MPa for 1 min uniaxial on the opposite side of the half-cell. For the pressure-dependent analysis the sodium WE is gradually pressed to the SE using uniaxial pressure. For dissolution experiments, symmetrical Na$_{id}$/NZSP0.4/Na$_{id}$ cells were prepared by contacting both sodium electrodes simultaneously to the SE using a uniaxial pressure of 11 MPa for 1 minute or an isostatic pressure of 100 MPa or 15 minutes.*

Table S-1: *List of the obtained binding energies for the measured signals in the Na 1s region for sodium metal under different measurement conditions. A detailed explanation of the measurement conditions can be found in Figure S6. The same color code as in Figure S6 was used. For sodium metal, besides the main signal Na^0, the first and second plasma excitation of bulk (B_{P1} and B_{P2}) and surface (S_{P1} and P_{S2}) are listed. In addition, the binding energy of the Na^+ signal is given, which describes an average BE including signals originating from SE and possible degradation products formed. A detailed description of the fitting model used can be find in section 4 in den supplementary information.*

Measuring condition	Calib. to	Na 1s region					
		Na^+	Na^0	Na^0 - B_{P1}	Na^0 - S_{P1}	Na^0 - B_{P2}	Na^0 - S_{P2}
Na on NZSP0.4	C 1s	1070.7	1069.2	1074.9	1073.2	1080.8	1079.0
Na on insulating tape	C 1s	-	1069.5	1075.3	1073.5	1081.1	1079.3
	E_F	-	1071.7	1077.5	1075.7	1083.6	1081.6
Na grounded	E_F	-	1071.8	1077.6	1075.8	1083.4	1081.6

Table S-2: *List of the determined binding energies (BE) and kinetic energies (KE) for the obtained signals in the O 1s region for sodium metal under different measurement conditions. A detailed explanation of the measurement conditions can be found in Figure S6. The same color code as in Figure S6 was used. For sodium metal, besides the main signal of Na^0-$KL_1L_{2,3}$, the first plasma excitation of bulk (B_{Plas}) and surface (S_{Plas}) are listed. In addition, the binding energy of the O1s signal is given, which describes an average BE including signals originating from SE and possible degradation products formed. A detailed description of the fitting model used can be find in section 4 in den supplementary information.*

Measuring condition	Calib. to	O 1s region						
		O1s	Na^0-$KL_1L_{2,3}$		Na^0-$KL_1L_{2,3}$ - $B_{Plas.}$		Na^0-$KL_1L_{2,3}$ - $S_{Plas.}$	
		BE	BE	KE	BE	KE	BE	KE
Na on NZSPO	C 1s	530.2	528.9	957.7	534.7	951.9	532.9	953.7
Na on insulating tape	C 1s	-	529.1	957.5	535.0	951.6	533.2	953.4
	E_F	-	531.4	955.2	537.2	949.4	535.4	951.2
Na grounded	E_F	-	531.4	955.2	537.3	949.3	535.5	951.1

Table S-3: *Absolute signal areas of Na 1s, O 1s, Zr 3d, Si 2p and P 2p of the solid electrolyte and immediately after sodium deposition and after 8 hours of retention time. Plasmons occurring in the Na 1s and O 1s region were not considered for the quantification.*

State of Sample	Na 1s/cps·eV	O 1s/cps·eV	Zr 3d/cps·eV	Si 2p/cps·eV	P 2p /cps·eV
Pristine	283.6	698.9	138.6	169.9	64.9
60 min	452.0	463.5	68.4	81.0	31.6
8 h	450.5	507.6	66.3	82.7	30.0

Table S-4: *Calculated activation energies of Na ion transport across different symmetrical cells with NZSP0.4 as solid electrolyte in the temperature range between − 40 and 40 °C. In addition to bulk and grain boundary, the total activation energy $E_{a,tot}$ for all cells was also determined. The abbreviation "id" indicates an ideally reversible electrode whereas "bc" indicates an electrode with low-load bearing contact. Even with small pores at the interface an ideal electrode behavior can be achieved. For the determination of the interfacial activation energy, insufficient contact was achieved by two different methods. For $E_{a,Int}$ highlighted in green, insufficient contact was achieved by anodic dissolution, whereas $E_{a,Int}$ highlighted in grey was determined by insufficient pressure during assembling.*

Activation energy	Au / NZSP0.4 / Au		Na_id / NZSP0.4 / Na_id	Na_id / NZSP0.4 / Na_id		Na_bc / NZSP0.4 / Na_id	
$E_{a,bulk}$ /eV	0.25(8)	0.25(8)	0.25(7)	0.25(2)	0.24(6)	0.25(7)	0.24(0)
$E_{a,GB}$ /eV	0.36(1)	0.34(0)	0.36(2)	0.37(0)	0.37(1)	0.36(2)	0.37(7)
$E_{a,tot}$ /eV	0.32(1)	0.31(2)	0.32(6)	0.32(4)	0.32(3)	0.32(9)	0.32(6)
$E_{a,Int}$ /eV	-	-	-	-	-	0.37(0)	0.38(1)

References

[1] S. Lunghammer, Q. Ma, D. Rettenwander, I. Hanzu, F. Tietz, H.M.R. Wilkening, *Chemical Physics Letters* **2018**, *701*, 147.

[2] J. T. S. Irvine, D. C. Sinclair, A. R. West, *Adv. Mater.* **1990**, *2*, 132.

[3] Q. Ma, C.-L. Tsai, X.-K. Wei, M. Heggen, F. Tietz, J. T. S. Irvine, *J. Mater. Chem. A* **2019**, *7*, 7766.

[4] S. Naqash, D. Sebold, F. Tietz, O. Guillon, *J. Am. Ceram. Soc*. **2019**, *102*, 1057.

[5] Richard J.D. Tilley, *Understanding Solids*. *The science of Materials*, John Wiley & Sons Inc., Chichester, **2013**.

[6] A. Barrie, F. J. Street, *Journal of Electron Spectroscopy and Related Phenomena* **1975**, *7*, 1.

[7] J. K. Eckhardt, P. J. Klar, J. Janek, C. Heiliger, *ACS Appl. Mater. & Interfaces* **2022**, *14*, 31, 35545-35554.